

A three dimensional in SILICO model for the simulation of inspiratory and expiratory airflow in humans

A.F. Tena, J.F. Francos, E. Álvarez & P. Casan

To cite this article: A.F. Tena, J.F. Francos, E. Álvarez & P. Casan (2015) A three dimensional in SILICO model for the simulation of inspiratory and expiratory airflow in humans, Engineering Applications of Computational Fluid Mechanics, 9:1, 187-198, DOI: 10.1080/19942060.2015.1004819

To link to this article: <http://dx.doi.org/10.1080/19942060.2015.1004819>



© 2015 The Author(s). Published by Taylor & Francis.



Published online: 20 Mar 2015.



Submit your article to this journal [↗](#)



Article views: 477



View related articles [↗](#)



View Crossmark data [↗](#)

A three dimensional *in SILICO* model for the simulation of inspiratory and expiratory airflow in humans

A.F. Tena^a, J.F. Francos^{b*} , E. Álvarez^b  and P. Casan^a

^aÁrea de Medicina, Departamento de Medicina, C/Julián Clavería, 6, 3^a planta, Campus del Cristo, 33006 Oviedo, Asturias, España;

^bÁrea de Ingeniería Hidráulica, Departamento de Energía, Universidad de Oviedo, Escuela Politécnica de Mieres. Universidad de Oviedo, C/ Gonzalo Gutiérrez Quirós s/n. 33600-Mieres, Asturias, España

(Received 1 September 2014; final version received 23 February 2015)

A three-dimensional, computational fluid dynamics model of the human respiratory system is put forward for consideration. This *in silico* model is based on existing state-of-the-art geometric approximations. As a complete simulation of the geometry would have unaffordable high computational costs, the model is composed of a single path of air from the mouth to the 16th bronchial generation, truncating the symmetrical branches that were not included. The innovation housed in this model is the development of a function that is applied to the truncated branches, which contemplates the behavior of the airflow within those branches, by copying cell by cell the velocity vectors existing in the symmetrical face of the developed branch. This model can reproduce the complete airflow process: inspiration and expiration cycles, through simulation in unsteady flow conditions. In normal breathing the air velocity varies within a narrow range, with steady changes. Therefore the model has been validated simulating a spirometry maneuver, in which an inspiration and expiration are performed in the most demanding conditions in order to obtain a wide speed range with faster variations.

Keywords: computational fluid dynamics; human respiratory system; inhalation; exhalation; spirometry

1. Introduction

For decades, mathematical models that reveal the morphology and workings of the human respiratory system have been developed. The first approaches were mainly focused on a mathematical description of the airways that make up the system.

The most commonly used anatomical model of the lower airways was developed by Weibel (1963). In this unidimensional model, the directions of bifurcation are indicated, designating the trachea as the first airway (generation 0) and assumed that each airway leads to two symmetrical branches (regular dichotomy). Weibel described a minimum of 23 bronchial generations up to the alveolar sacs, specifying lengths and diameters. Alternative approaches based on Weibel's morphology, which enhance the description of the lungs, have been proposed. The most notable are the work by Horsfield and Cumming (1968) who introduced some asymmetries in the model, modifying the diameter of the airways and the branching angles; and the morphology developed by Hammersley and Olson (1992) which is suitable for the smaller airways (from generations 6 to 12).

Other research work carried out focus on detailed mathematically descriptions of the airways: Sauret, Goatman, Fleming, and Bailey (1999) and Hegedüs, Balásházy, and

Farkas (2004) and Schmidt, Zidowitz, Kriete, Denhard, Krass, and Pietgen (2004) proposed high-resolution models of morphologically lifelike airways up to the fifth bronchial generation; Kitaoka, Takaki, and Suki (1999) and Tawhai and Burrowes (2003) proposed algorithmic techniques to describe the geometry of the lower airways.

More recently, the use of computational fluid dynamics (CFD) modeling techniques and the increased calculation capacity of computers have facilitated the modeling and simulation of the airflow throughout the airways. However, few studies to date have attempted to simulate the flow in the whole airway or even through the conducting airways: it can be deduced from the basic morphology of Weibel (1963) that the number of paths for the airflow in the conducting airways is equal to 2 to the power of 23, i.e., more than 8 million individual flow segments. A computational resolution of the complete flow at all scales with pinpoint accuracy would require a mesh size of the order of several billions of elements, making it impossible to simulate with existing computer capabilities.

A first attempt to solve this problem was made by Nowak, Kadake, and Annapragada (2003). Nowak used a series of increasingly smaller models of the airways. An entry boundary condition obtained from a simulation of the section immediately above was applied to each section of

*Corresponding author. Email: jffrancos@uniovi.es

the airways. One of the difficulties that arises in this type of sequential procedure is that the output boundary condition at the end of each section must be prescribed before running calculations. The authors found that an equal mass division in the outlets was more appropriate as a boundary condition than a constant pressure value. A similar methodology was applied by Zhang, Kleinstreuer, and Kim (2008) to simulate a model based on Weibel's model. Although both studies represented a significant advance in the simulation of the airflow in the lungs, this sequential procedure does not allow a full-flow coupling at all levels.

Later, researchers opted for a partial resolution of the airway geometry to perform a continuous 3D Computational Fluid Dynamics (CFD) simulation. In these cases only a reduced number of the flow paths were taken into account, providing identical conditions at the areas that were not modeled.

The first significant approach to apply a reduction in the number of resolved flow paths was the work of Gemci, Ponyavin, Chen, Chen, and Collins (2008), which uses the seventeen-generation lung model of Schimdt et al. (2004). The authors studied the inhalation process in a reduced number of resolved flow paths from trachea (generation 0) up to the terminal bronchioles (generation 17), through quasi steady-state simulations. An equal and constant pressure condition at all flow outlets (corresponding to areas not modeled) has been used.

The current state of the art for CFD simulations is the use of partially resolved models of the lung airways, in which some branches are removed (truncated) from the airway tree at different levels of the scale. The truncated branches are substituted by boundary conditions. The challenge is to provide realistic conditions for these geometries.

In keeping with such criteria, Walters and Luke (2010) uses Weibel's morphology and the anatomical data of Hammersley and Olson, truncating 50% of the airway paths in each generation from the second generation (bronchi) to the twelfth generation (bronchioles) to create steady state simulations of the inhalation process. The truncations were executed in the middle of the branch segment and a calculated value of static pressure was used as a boundary condition. This pressure value is obtained using a probabilistic approach using pressure data from resolved flow paths. In another paper (Walters, Burgreen, Lavalley, Thompson, & Hester, 2011), the authors continue the investigations of the airflow in steady state conditions using the same static pressure calculation approach for truncated branches in a CT based model. Later on, Walters, Burgreen, Hester, Thompson, Lavalley, Pruet, and Ford-Green (2012), using the same model, presents the results obtained in a complete breathing cycle using unsteady-state simulations, where boundary conditions at truncated branches are prescribed based on an presupposed mass flow split at each bifurcation (it assumes uniform velocity profile).

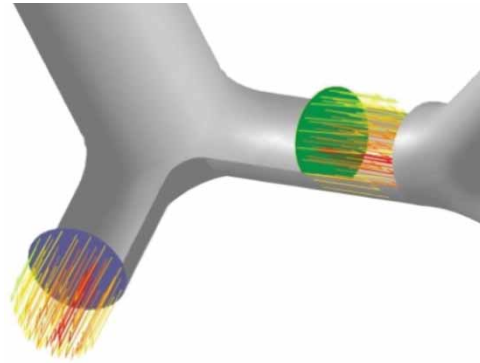


Figure 1. Velocity vectors in the exit of the truncated branch (marked in blue colour) and its symmetrical face in the opened airway (marked in green colour).

Another approach to simplify the complete lung model is to define a single-path model. This was indicated by Spencer, Schroeter, and Martonen (2001) as a way to optimize computational costs in simulations with realistic airway surface features. Longest also demonstrated that the approach including a stochastic individual path (SIP) CFD model from the secondary bronchi to the terminal bronchioles (Tian, Longest, Su, Walenga, & Hindle, 2011) permits accurate studies of the transport and deposition of pharmaceutical aerosols from inhalers (Tian, Hindle, & Longest, 2014). The authors specify mass flow rate boundary conditions at truncated outlets, based on a presupposed even split of the air flow at each bifurcation.

Following the single-path approach, this paper endeavors to provide an investigation that includes a model combining existing CT-based geometries of the upper airways (nose, mouth and throat) with a designed single-path model from the trachea up to the terminal bronchioles. The branches are symmetric, based on the geometries proposed by Weibel and Kitaoka. This symmetrical state allows the use of a boundary condition for each simulation step that imposes the same velocity vector field in the truncated-branches as in the developed branches through which the air-flow passes (Figure 1). This boundary condition is considered much more realistic than predefined flow-rate values or pre-calculated pressure conditions. The model is validated with a complete spirometry test which represents the most demanding conditions for unsteady simulations of both the inhalation and exhalation cycles.

2. DEVELOPED MODEL

2.1. The basis

For the elaboration of the three-dimensional airway model, the model proposed by Kitaoka et al. (1999) is combined with Weibel's model (1963).

Weibel's classic model indicates the bifurcation modes, designing the trachea as the first airway (order 0) and assuming that each airway generates two new branches (regular dichotomy). Thus, the left and right main bronchi

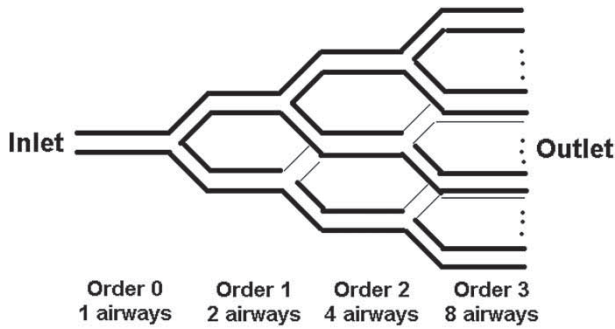


Figure 2. Airway scheme.

are order 1 and so on. There are at least 23 airway generations until reaching the alveolar sacs. In accordance with this model, there is one order 0 generation ($2^0 = 1$), 2 airways of order 1 ($2^1 = 2$), 4 airways of order 2 ($2^2 = 4$), etc. Therefore there are 2^{23} airways of order 23; the number of ramifications increases exponentially to a total of 8,388,608 (2^{23}). Figure 2 shows a scheme of these airways.

The diameter of each ramification diminishes according to the formula $d_n = d_0 \cdot 2^{-1/n}$, n represents the generation order and d the diameter. This relationship is maintained up to generation 16 at the end of the conductive zone. From generation 17 to 23 there are only small changes in the dimensions of the airways, because they are more or less alveolized. In Weibel's model the spatial disposition of the branches was not taken into account, therefore it only allows one-dimensional modeling of the lung.

Kitaoka et al. (1999) brought about the design of a realistic three dimensional model of the lung, with nine basic rules:

- Rule 1: Branching is dichotomous.
- Rule 2: The parent branch and its two daughter branches lie on the same plane, called the branching plane.
- Rule 3: The volumetric flow rate through the parent branch is conserved after branching; that is, the sum of the flows in the daughter branches is equal to the flow in the parent branch.
- Rule 4: The region supplied by a parent branch is divided into two daughter regions by a plane called the "space-dividing plane." The space-dividing plane is perpendicular to the branching plane and extends out to the border of the parent region. There is a supplementary rule (rule 4a) for correcting the space division scheme whenever the space in that region requires it.
- Rule 5: The flow-dividing ratio "r" is set to be equal to the volume-dividing ratio, defined as the ratio of the smaller daughter region to that of its parent. Figure 3 illustrates these rules.

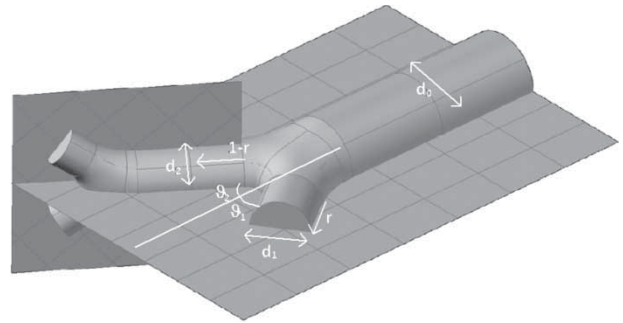


Figure 3. Three dimensional model of the lung proposed by Kitaoka.

- Rule 6: Diameters and branching angles of the two daughter branches are determined by substituting r from rule 5 into the following equations.

With no symmetry:

$$d_1 = d_0 r^{1/n}, d_2 = d_0 (1 - r)^{1/n}$$

$$\cos\theta_1 = \frac{1 + r^{4/n} - (1 - r)^{4/n}}{2r^{2/n}};$$

$$\cos\theta_2 = \frac{1 - r^{4/n} + (1 - r)^{4/n}}{2(1 - r)^{2/n}}$$

With symmetry:

$$\theta_1 = \theta_2; r = 1/2; d_1 = d_2 = d_0 2^{-1/n}; \cos\theta = 2^{(\frac{2}{n}-1)}$$

Where:

- d is the airway diameter
- subindex 0 for mother branch
- subindexes 1 and 2 for daughter branches
- n is a constant called diametrical exponent (for laminar flow its value is 3 and for turbulent flow its value is 2.6)

There is a supplementary rule (rule 6a) to correct the branching angle according to the shape of the daughter region.

- Rule 7: The length of each daughter branch has a value three times its diameter. There is a supplementary rule (7a) to correct the length according to the shape of the region.
- Rule 8: If branching continues in a given direction, the daughter branch becomes the new parent branch, and the associated branching plane is set perpendicular to the branching plane of the old parent. There is a supplementary rule (8a) to correct the rotation angle according to the shape of the region.

- Rule 9: The branching process in a given direction stops whenever the flow rate becomes less than a specified threshold or the branch extends beyond its own region.

2.2. Geometric model

The geometric model used is composed of a conductive airway model designed following Weibel's (1963) and Kitaoka's et al. (1999) symmetrical cases, as well as existing upper airways models. It was developed up to the 16th bronchial generation (end of the conductive airways) because, according to Weibel's model, from the 17th generation to the end, the airways are alveolized. The development of the geometry of the alveolar units is much more complex and is beyond the scope of this work.

a) Conductive airways model

The numerical model of the conductive airways was designed to be as realistic as possible while avoiding prohibitive computational costs when it is simulated. Therefore the model has been simplified in two ways:

1. Considering a model of a single active branch: when the trachea divides into the two main bronchi, the model will continue through the right main bronchus while the pathway through the left main bronchus will be "truncated." When the right main bronchus bifurcates into the right upper bronchus and the intermediate bronchus, the model will continue through the intermediate bronchus and the upper right bronchus will be "truncated," and so on. This kind of model was researched and developed by Walters and Luke (2010) and Walters et al. (2012) and has proven to be effective to simulate the entire lung, saving time and computational costs.
2. Overlooking the changes in the diameter of the airway in accordance with the respiratory-cycle phase.

The diameter and the length of the airways were deduced from the relations proposed by Weibel (1963) and Kitaoka et al. (1999):

$$d = 0.018^{-0.388n}; l = 0.012^{-0.92n} \text{ if } n \leq 3$$

$$d = 0.013^{-(0.2929-0.00624n)n}; l = 0.025^{-0.17n} \text{ if } n > 3$$

Being, d the airway diameter, n the generation order and l the airway length.

A summary of the main geometric dimensions in the branches is presented in Table I.A (see Annex).

With this data and other restrictions from Weibel's (1963) and Kitaoka's et al. (1999) model, the geometry was constructed using the commercial software Ansys Gambit 2.4.6. The numerical model of the lung, composed of an open branch (or single path), is shown in Figure 4. The complete morphology of the lung can be generated from

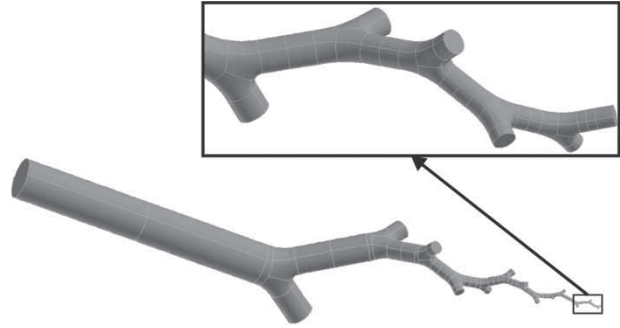


Figure 4. Geometric model of the lung.

the numerical model. This can be done by establishing symmetry at each of the truncated branches.

b) Upper airways model

Once the model has been designed up to the 16th bronchial generation, the next step is to complete the conductive airway by adding the upper airway components: nose, mouth and throat (larynx and pharynx).

The nose is constructed using the simplified geometrical model used in Castro-Ruiz (2003) obtained from CT images of a thirty-year-old woman. The volume of each duct of the nose is 19,568 mm³. Figure 5 shows the model used (right image) and seven coronal cuts (left image), with the following areas: 1: 482 mm², 2: 205 mm², 3: 164 mm², 4: 198 mm², 5: 154 mm², 6: 33 mm² and 7: 13 mm². The perimeter of the cuts allows the construction of the longitudinal surfaces using the following distances between sections: 1 – 2: 18 mm, 2 – 3: 10 mm, 3 – 4: 36 mm, 4 – 5: 16 mm, 5 – 6: 17 mm and 6 – 7: 7 mm.

The mouth and throat are a reproduction of the Stapleton model (Stapelton, Guentsch, Hoskinson, & Finlay, 2000) constructed by using simple geometric shapes. The advantage of this approach is that extremely high mesh resolutions are not needed near the walls to resolve all the small airway irregularities.

The geometry of the mouth used is shown in Figure 6. In the left image seven coronal cuts in the mouth model (right image) are shown. The areas are: 1: 503 mm², 2: 471 mm², 3: 574 mm², 4: 638 mm², 5: 653 mm², 6 and 7: 257 mm². The distances between sections are: 2–3: 25 mm, 3–4: 25 mm, 4–5: 30 mm, 5–6: 4 mm and 6–7: 11 mm. The walls of the mouth are smoothly joined with the walls of the pharynx. The shape of the tongue changes while speaking or swallowing. This model has a flat tongue in the foremost part of the mouth.

The throat geometry is more complicated because its three points of entry (two nasal passages, the choanae; and the mouth passage, the fauces) become a single conduct (the pharynx) whose output is the trachea. Inside this conduct is the epiglottis, a cartilage separating the trachea from the esophagus. The epiglottis is smoothly attached to the trachea. The epiglottal folds form a tube with a diameter of approximately 18 mm.

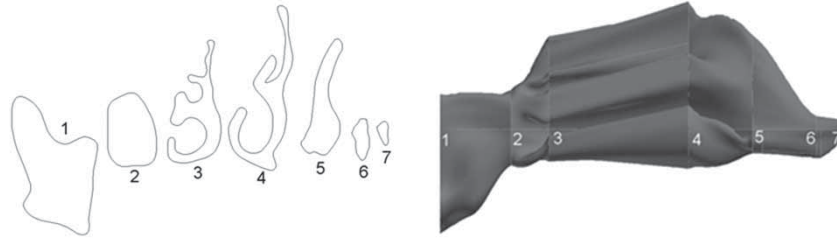


Figure 5. Geometry of the nose.

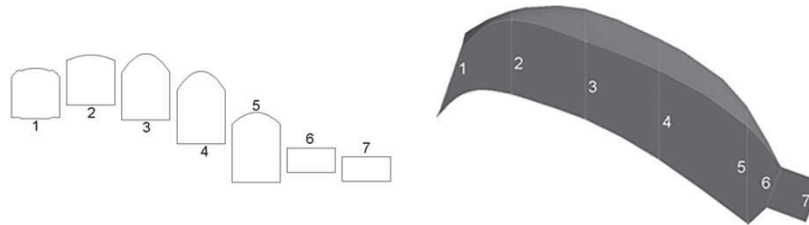


Figure 6. Geometry of the mouth.

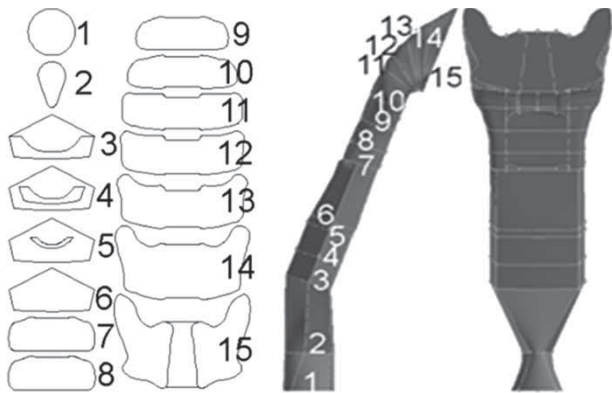


Figure 7. Geometry of the throat.

Figure 7 represents the throat model (right image) divided into sections (left image). The pharynx includes cross sections from 7 to 15, with the corresponding areas: 7: 393 mm², 8: 391 mm², 9: 392 mm², 10: 458 mm², 11: 572 mm², 12: 658 mm², 13: 752 mm², 14: 1020 mm² and 15: 964 mm². The larynx includes cross sections from 1 to 6 with the corresponding areas: 1: 254 mm², 2: 126 mm², 3: 242 mm², 4: 315 mm², 5: 370 mm² and 6: 395 mm².

The entire geometric airways model is presented in Figure 8.

2.3. Numerical model

Once the geometry has been done, the next step is to create the numerical model. This is determined by dividing, or meshing, the geometry into different cells in which the flow equations must be solved. Therefore a mesh will be applied, choosing the appropriate cell type.

a) Meshing



Figure 8. Geometric airways model.

The model of the lung was meshed with tetrahedral cells because of their favorable adaptation to complex geometries. The size of the tetrahedrons diminishes while descending from high-order to low-order generations. Before meshing the volumes a boundary layer mesh was built using structured meshing in order to obtain a better description of the boundary layer in the numerical calculations. The size of the tetrahedrons was consistent with the size of the boundary layer cells.

The total size of the grid is about 10⁶ cells. A quality analysis of the mesh yielded very satisfactory results, indicating a magnitude of the equitize skew below 0.6 for 98% of the cells in the mesh. This parameter shows the shape of the cells formed. Values near 0 indicate more regular cells,

which have a higher probability of obtaining satisfactory results.

Figure 9 shows an example of the surface mesh at some branches with a detail of the boundary layer mesh that includes numerical information needed for its definition. The boundary mesh has equal number of cells for each branch as the number of rows (6rows) and other dimensionless parameters are evenly set throughout the model.

b) Flow equations

The equations that describe a fluid (air in this case) in movement can be deduced from the mass and momentum conservation laws. Applying these conservation laws to an incompressible fluid element, the Navier-Stokes equations are obtained:

Continuity:

$$\nabla \cdot \vec{v} = 0$$

Momentum:

$$\rho \frac{d\vec{v}}{dt} = -\nabla p + \rho \vec{g} + \mu \nabla^2 \vec{v}$$

where:

- \vec{v} is the air velocity.
- p is the air pressure.
- μ is the dynamic viscosity of the air.
- ρ is the air density
- \vec{g} is the constant gravity

Resolving these equations by using a turbulence model, the values of pressure and velocity of the fluid in each cell may be obtained.

c) Boundary conditions

To solve the flow equations in the inhalation and exhalation cycles, a set of boundary conditions have been selected.

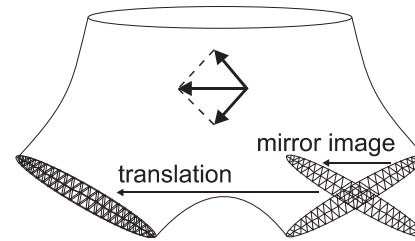


Figure 10. UDF for truncated branch.

- Mouth (model inlet) and 16th bronchial generation (model outlet): values of static pressure, total pressure (sum of static and dynamic pressures) or flow rate conditions have been used depending on the test carried out.
- Truncated branches conditions: these need a special boundary condition because the same conditions which were imposed at the inlet and outlet of the model cannot be applied. This special condition must unwaveringly represent the effect of the branches removed. A user-defined function (UDF) is used to impose a symmetric operation of two branches. This UDF obtains the velocity vector field at each open branch (either in inhalation or exhalation) from the calculations, and prescribes the same vector field in the corresponding truncated branch (Figure 10). This methodology is repeated repeatedly until reaching convergence in the flow field.

d) Solution parameters

The numerical calculations were resolved with the commercial code Ansys Fluent 6.3.26. This code was used to solve the unsteady Reynolds-averaged Navier-Stokes

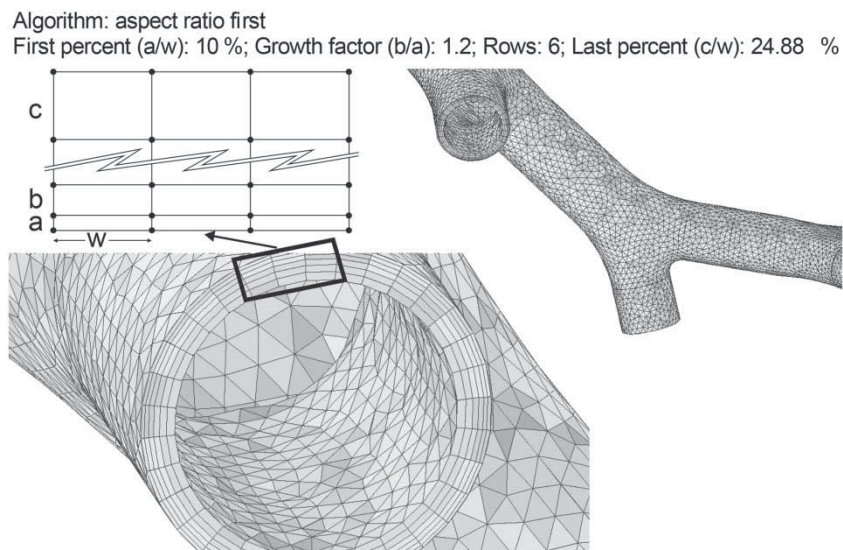


Figure 9. Surface meshes at some branches: a detail of the boundary layer mesh.

equations (URANS) by the finite volume method, converting them from differential equations into their numerical analogues (Eulerian method).

The solutions were obtained, assuming air with a constant density 1.225 kg/m^3 and dynamic viscosity $1.9 \times 10^{-5} \text{ kg/m s}$.

The SIMPLE (Semi-Implicit Method for Pressure Linked Equations) algorithm was used to resolve the coupling between pressure and velocity fields, the same solver used by Walters in his research (Walters & Luke, 2010 and Walters et al., 2012). The discretization of the spatial and temporal derivatives for the velocities in the equations was carried out by means of second-order schemes. The PRESTO! discretization scheme was used for the pressure.

Since the flow in human airways is both laminar and turbulent, with transition zones, the turbulence model chosen for this work is the shear stress transport $k-\omega$ (SST $k-\omega$), which is the best suited to these conditions. While the standard $k-\omega$ turbulence model performs better than $k-\varepsilon$ in the near wall region, it is worse in the far field; this is why the shear stress transport formulation has been selected: it combines the best of both (Versteeg & Malalasekera, 2007). The SST $k-\omega$ model is defined by the following two equations:

$$\begin{aligned} \frac{\partial}{\partial t}(\rho k) + \frac{\partial}{\partial x_i}(\rho k u_i) &= \frac{\partial}{\partial x_j} \left(\Gamma_k \frac{\partial k}{\partial x_j} \right) + \tilde{G}_k - Y_k + S_k \\ \frac{\partial}{\partial t}(\rho \omega) + \frac{\partial}{\partial x_i}(\rho \omega u_i) &= \frac{\partial}{\partial x_j} \left(\Gamma_\omega \frac{\partial \omega}{\partial x_j} \right) + G_\omega - Y_\omega \\ &+ D_\omega + S_\omega \end{aligned}$$

Where k is the turbulence kinetic energy; ω is the specific dissipation rate; ρ is the air density; \tilde{G}_k represents the generation of turbulence kinetic energy due to mean velocity gradients; G_ω represents the generation of ω ; Γ_k and Γ_ω represent the effective diffusivity of k and ω respectively; Y_k and Y_ω represent the dissipation of k and ω due to turbulence; D_ω represents the cross-diffusion term and S_k and S_ω are user-defined source terms.

3. SIMULATION METHODOLOGY

The designed model has been validated by two tests: a first test in which a real spirometry is introduced in the model and a second test used to check the results obtained in the first one. A forced spirometry test has been used for the evaluation of the model as it presents the maximum variations of flow rate possible. Therefore the model is tested in the most challenging conditions.

Different forced spirometry tests of individuals without obstructive pulmonary diseases were performed to obtain data under realistic conditions. The spirometry that best matched the ERS (European Respiratory Society) quality criteria was chosen (Miller, Hankinson, Brusasco, Burgos, Casaburi, Coates, Crapo, Enright, van der Grinten,

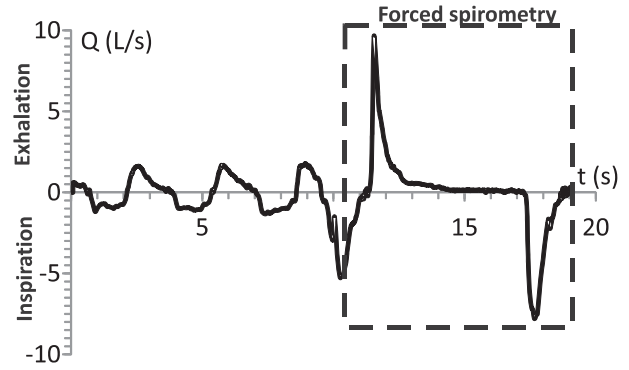


Figure 11. Relationship between flow rate and time from the chosen spirometry.

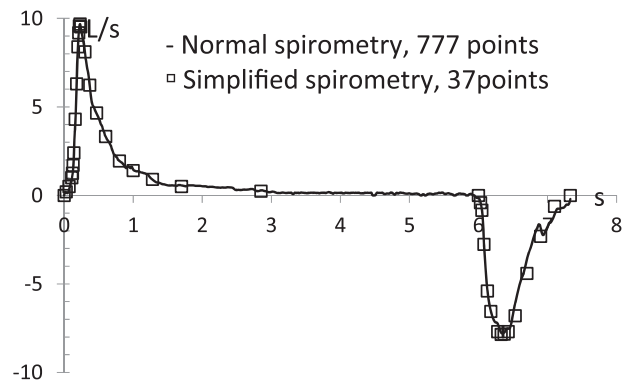


Figure 12. Normal and simplified spirometry.

Gustafsson, Jensen, Johnson, MacIntyre, McKay, Navajas, Pedersen, Pellegrino, Viegi, & Wanger, 2005). The spirometry data was obtained using a spirometer model CPFS/D USB, with a MedGraphicspreVentTMPneumotachometer and BREEZESUITETM diagnostic software (Medical Graphics Corporation 2004, 350 OakGrove Parkway, St. Paul, Minnesota 55127–8599).

In a spirometry test the spirometer measures pressure differences in a venturi tube during the test period. Then a software tool calculates the time evolution of the mean velocity and the flow rate. The relationship between the flow rate and time is represented in Figure 11. From this data, the portion corresponding to the forced spirometry corresponds to the data obtained between seconds 11.32 and 19.09.

For calculation purposes the original spirometry has been simplified, reducing the number of points from 777 to 37 and adjusting the new curve (Figure 12). The number of points has been reduced to include the important changes in the inlet flow so that the simulation is not overburdened with irrelevant tasks.

To reproduce the same conditions as in a real spirometry, the boundary conditions values used/adopted imposed were:

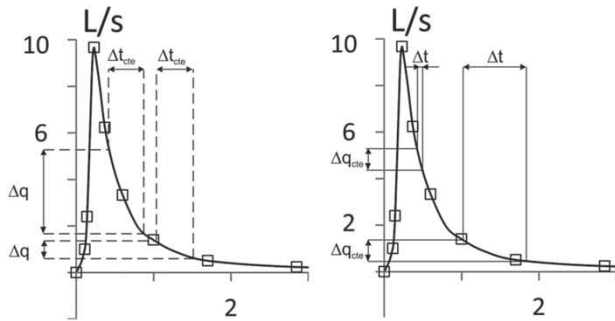


Figure 13. The graph on the left shows the option with a constant time step (variable flow rate step), the graph on the right shows the option with a constant flow rate step (variable time step).

- Mouth (inlet): flow rate varying over time using the detailed function, and atmospheric pressure. During the respiratory cycle (inhalation and exhalation) the inlet of the model, the source of the trachea, is set at atmospheric pressure. In fact, it is slightly lower as it has to pass through the mouth. However, this does not affect the calculations. In order to apply the values of the flow rate obtained in the spirometry to the model, it was necessary to design a user-defined function (UDF) as Ansys Fluent has no established functions to simulate time-dependent variables. Due to the non-uniformity of the breathing cycle and in order to include all the representative points, this UDF must include a subroutine to adapt the magnitude of the time step to a calculated percentage of change in the flow rate (adaptive time step). This value is also calculated by the UDF using the data of the number of steps defined and the spirometry function (Figure 13). The UDF automatically changes the conditions from inhalation to exhalation.
- 16th bronchial generation (outlet): a static pressure in the inhalation cycle and a total pressure (sum of static and dynamic pressures) in the exhalation cycle (Figure 14).

Finally, to check the previous test and the results found, the unsteady pressure function obtained was set as the inlet boundary condition at the 16th bronchial generation. Figure 15 shows the new boundary conditions employed:

- Mouth (inlet): static pressure on the exhalation cycle and a total pressure on the inhalation cycle.
- Sixteenth bronchial generation (outlet): a total pressure (sum of static and dynamic pressures) varying over time using the same function (UDF) that was used to introduce the variable flow rate in the previous test.

The convergence criterion established was to reduce the scaled residuals for all the variables below 10^{-5} . One

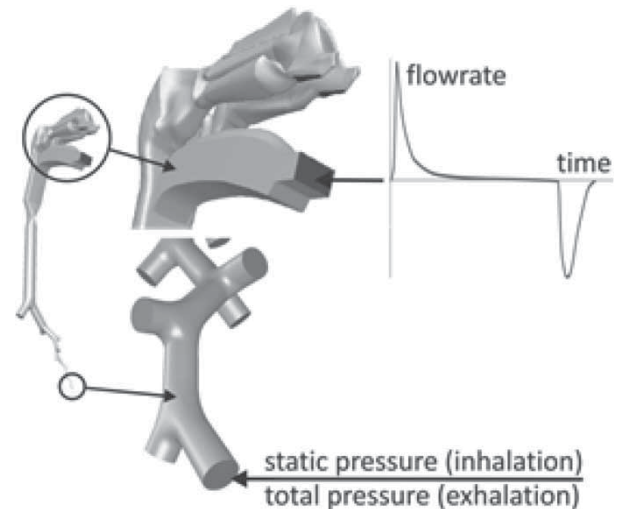


Figure 14. Boundary conditions imposed in the first test.

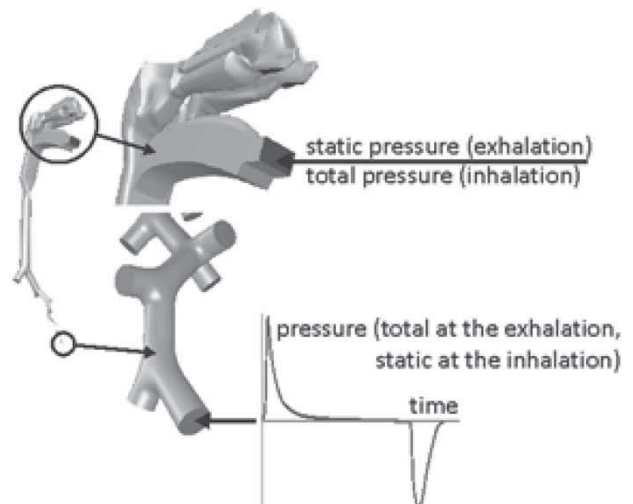


Figure 15. Boundary conditions established at the checking test.

thousand steps were used. A maximum of 1,400 iterations were required in order to ensure the convergence of the results at each time step. The spirometry maneuver in forced conditions was covered in 1000 flow steps with the corresponding time adaptations.

4. RESULTS AND DISCUSSION

With these values the time required for each simulation was 5 days working in parallel on a computer with an I-7 processor of 8 cores. The results of the tests provide data of the lung that cannot be obtained with a real forced spirometry. For example, Figure 16 shows static pressure obtained at the 16th bronchial generation of the lung as result of the first test. It is compared with the boundary condition used (unsteady flow rate obtained from the chosen forced spirometry test) finding that the static pressure curve at the 16th bronchial generation obtained has a similar tendency

to the one of the flow rate curve. This indicates a suitable performance of the numerical model.

Upon further examination and checks carried out, it was noticeable how different variables (pressures and velocities) have similar values in both cases, meaning that the solutions are unique and representative for the inhalation and exhalation cycles. For example, Figure 17 shows that the maximum velocity occurs at time 0.23 s, being 38.02 m/s the value obtained experimentally and 37.04 m/s the simulated value. Therefore, the maximum error is less than 2.6%.

The contours of the instantaneous static pressure and velocity vector field during inhalation are shown in Figure 18 and Figure 19. It can be observed that the magnitude of the pressure drops from the mouth (zero pressure) to the narrow area close to the glottis where a minimum of about -3.6×10^{-3} Pa is obtained. This corresponds to an increase in velocity from 0 m/s (in the mouth) to a maximum value of around 45 m/s in the mentioned area. After this section, the air velocity descends in the trachea, and from the trachea the velocity increases again up to a maximum value around 35 m/s at the third level and therefore a reduction in the static pressure is produced. For the following generations the velocity decreases as the lung

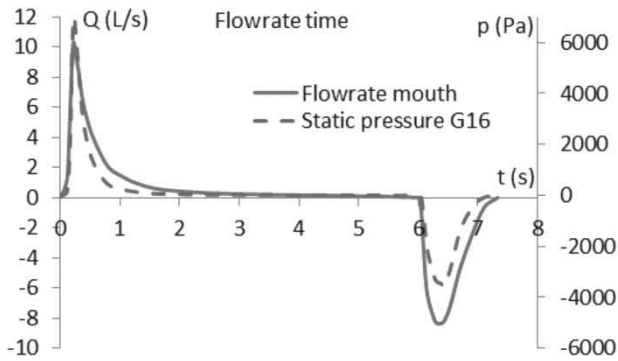


Figure 16. Unsteady flow rate established at the mouth in the simulation whilst static pressure is obtained in the 16th bronchial generation.

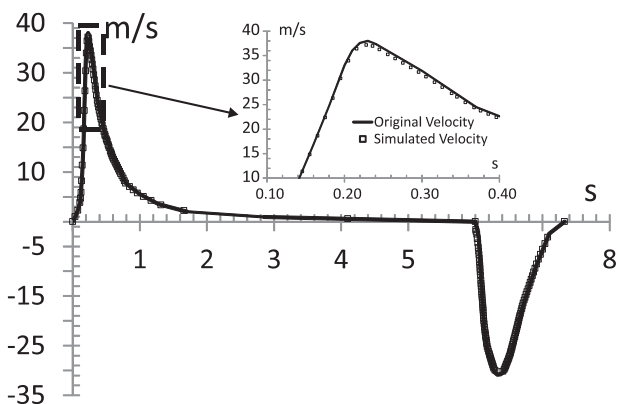


Figure 17. Real and simulated velocities at the mouth.

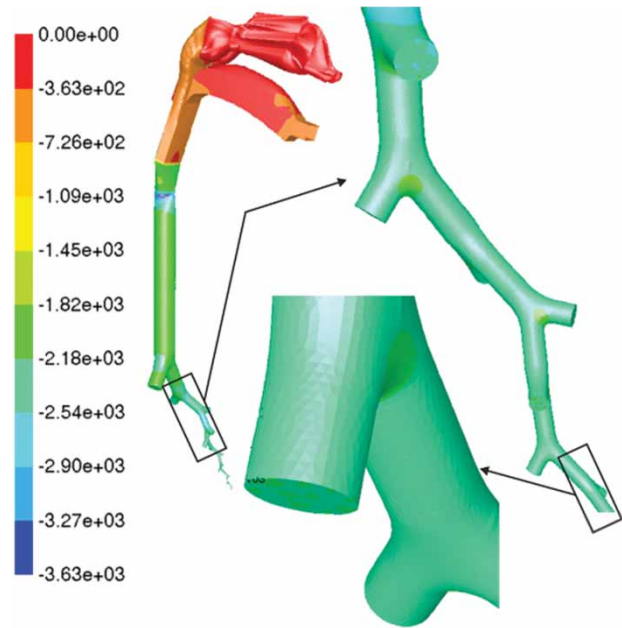


Figure 18. Pressure contours at maximum inhalation flow rate (Pa).

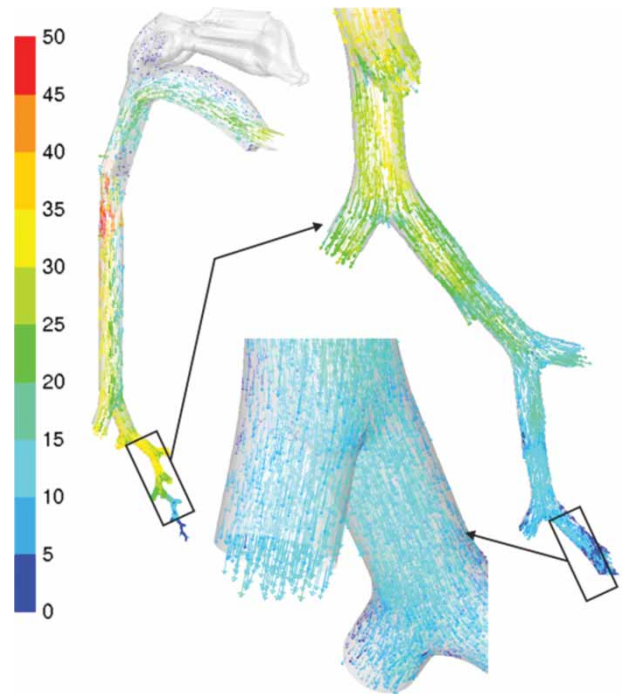


Figure 19. Velocity vector field at maximum inhalation flow rate (m/s).

surface increases, though there is no appreciable variation in terms of pressure.

The contours of the instantaneous static pressure during exhalation are shown in Figure 20. As one may observe, the magnitude of the pressure diminishes while ascending from the lowest generation to the trachea, where a magnitude of zero pressure is reached (i.e., atmospheric

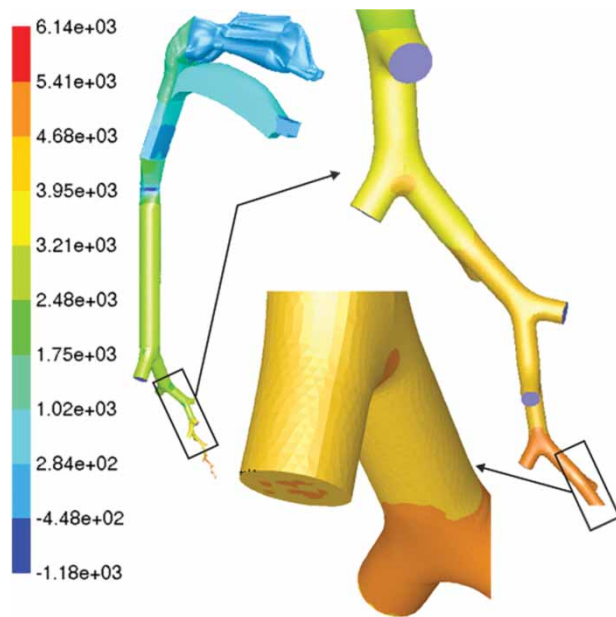


Figure 20. Pressure contours at maximum exhalation flow rate (Pa).

conditions). The symmetry of the velocity field at the bifurcations may also be noted. As expected, the velocity has maximum values in the area close to the glottis and the 3rd level (around 50 m/s). The velocity decreases from the third level to the trachea as the surface of the lung increases in the flow direction (Figure 21) while from other levels to third the velocity gradually increases since there is an overall decrease in the lung's surface. This explains the reduced pressure in the different zones (Figure 20, Figure 21). These results comply with those already quoted Sbirlea-Apiou, Katz, Caillibotte, Martonen and Yang (2007) and Gemci, Ponyavin, Chen, Chen & Collins (2008).

Using post processing data, two typical parameters that describe turbulence modeling: y^+ and a Reynolds number (Re), have been obtained. With regard to the near-wall resolution, the average value of y^+ obtained was 0.91. Reynolds numbers in the range of 0–8700 for normal breathing and 0–47,000 for spirometry tests were found. The maximum values correspond to the conditions in the trachea (diameter of 0.018 m) with velocity ranges of between 0–7 m/s (normal breathing) and 0–38 m/s (spirometry test) respectively.

5. CONCLUSION

This paper reveals a three-dimensional *in silico* CFD model of the human airways designed following Weibel's and Kitaoka's symmetrical models as well as existing upper airways models. It consists of a single air path from the mouth to the 16th bronchial generation in addition to a user-defined-function (UDF) that represents the effect of the branches that were not contemplated. The UDF copies cell by cell the velocity vectors existing in the cross section of

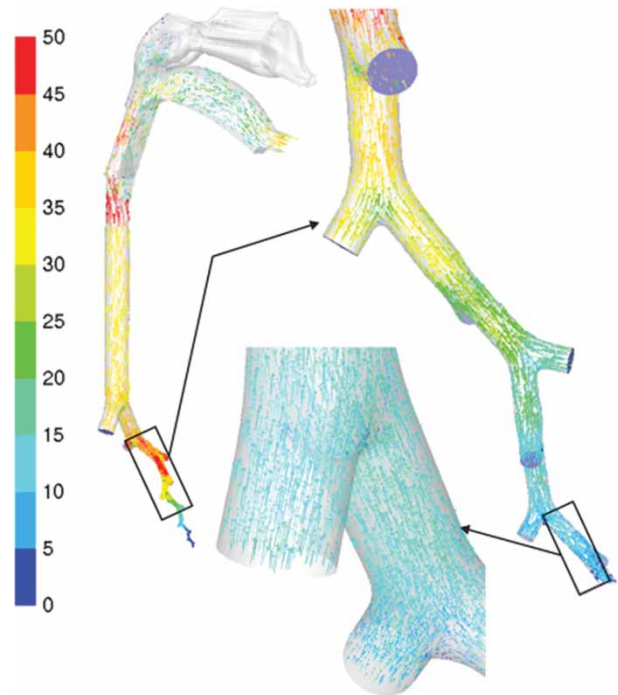


Figure 21. Velocity vector field at maximum exhalation flow rate (m/s).

a developed branch to the symmetrical truncated one while consolidating simulation. This approach permits a continuous unsteady simulation of the respiratory system both in the inspiration and the exhalation cycles, using limited computational resources, making it affordable.

In the investigations, in order to achieve a fully reliable CFD simulation, the airway model was meshed using 10^6 tetrahedral cells, which offer satisfactory results with a suitable adaptation to the geometry. The model has been validated using flow data of a real forced spirometry. This involved introducing the flow rate values through the model inlet (mouth) with a user-defined function designed for this purpose. The results were very lifelike values of pressure and velocity at all airways levels. These results were checked by applying the reverse conditions to the model (total pressure in the outlet of the model at 16th bronchial generation) thereby obtaining similar results to those of the spirometry test.

Further research work could be carried out with the model obtained in order to investigate specific diseases, such as chronic bronchitis and lung emphysema, as well as the study of the deposition of pollutants or drugs in the airways.

ORCID

J.F. Francos  <http://orcid.org/0000-0003-1495-9848>

E. Álvarez  <http://orcid.org/0000-0003-4585-9911>

References

- Castro-Ruiz, P. (2003). *Análisis computarizado del flujo aéreo en cavidad nasal* [Thesis doctoral]. Universidad Autónoma de Madrid.
- Gemci, T., Ponyavin, V., Chen, Y., Chen, H., & Collins, R. (2008). Computational model of airflow in upper 17 generations of human respiratory tract. *Journal of Biomechanics*, 41, 2047–2054.
- Hammersley, J., & Olson, D. (1992). Physical models of the smaller pulmonary airways. *Journal of Applied Physiology*, 72(6), 2402–2414.
- Hegedüs, C. J., Balásházy, I., & Farkas, Á. (2004). Detailed mathematical description of the geometry of airway bifurcations. *Respiratory Physiology & Neurobiology*, 141(1), 99–114.
- Horsfield, K., & Cumming, G. (1968). Morphology of the bronchial tree in man. *Journal of Applied Physiology*, 24(3), 373–383.
- Kitaoka, H., Takaki, R., & Suki, B. (1999). A three-dimensional model of the human tree. *Journal of Applied Physiology*, 87, 2207–2217.
- Miller, M. R., Hankinson, J., Brusasco, V., Burgos, F., Casaburi, R., Coates, A., ... Wanger, J. (2005). Standardisation of spirometry. *European Respiratory Journal*, 26, 319–338.
- Nowak, N., Kadake, P. P., & Annapragada, A. V. (2003). Computational fluid dynamics simulation of airflow and aerosol deposition in human lungs. *Annals Biomedical Engineering*, 31(4), 374–390.
- Sauret, V., Goatman, K. A., Fleming, J. S., & Bailey, A. G. (1999). Semi-automated tabulation of the 3D topology and morphology of branching networks using CT: application to the airway tree. *Physics in Medicine and Biology*, 44(7), 1625–1638.
- Sbirlea-Apiou, G., Katz, I., Caillibotte, G., Martonen, T., & Yang, Y. (2007). Deposition mechanics of pharmaceutical particles in human airways (2007). *Lung Biology in Health and Disease*, 221, 1–30.
- Schmidt, A., Zidowitz, S., Kriete, A., Denhard, T., Krass, S., & Pietgen, H. O. (2004). A digital reference model of the human bronchial tree. *Computerized Medical Imaging and Graphics*, 28(4), 203–211.
- Spencer, R. M., Schroeter, J. D., & Martonen, T. B. (2001). Computer simulations of lung airway structures using data-driven surface modeling techniques. *Computers in Biology and Medicine*, 31(6), 499–511.
- Stapelton, K. W., Guentsch, E., Hoskinson, M. K., & Finlay, W. H. (2000). On the suitability of the κ - ϵ turbulence modeling for aerosol deposition in the mouth and throat: a comparison with experiment. *Journal of Aerosol Science*, 31, 739–749.
- Tian, G., Longest, P., Su, G., Walenga, R. L., & Hindle, M. (2011). Development of a stochastic individual path (SIP) model for predicting the tracheobronchial deposition of pharmaceutical aerosols: effects of transient inhalation and sampling the airways. *Journal of Aerosol Science*, 42(11), 781–799.
- Tian, G., Hindle, M., & Longest, P. W. (2014). Targeted lung delivery of nasally administered aerosols. *Aerosol Science and Technology*, 48(4), 434–449.
- Tawhai, M. H., & Burrowes, K. S. (2003). Developing integrative computational models of pulmonary structure. *Anatomical Record*, 275B(1), 207–218.
- Versteeg, H. K., & Malalasekera, W. (2007). *An introduction to computational fluid dynamics*. Harlow, England: Pearson.
- Walters, D. K., & Luke, W. H. (2010). A method for three-dimensional Navier-Stokes simulations of large-scale regions of the human lung airway. *Journal of Fluids Engineering*, 132(5), 051101-1–051101-8.
- Walters, D. K., Burgreen, G. W., Lavalley, D. M., Thompson, D. S., & Hester, R. L. (2011). Efficient, physiologically realistic lung airflow simulations. *Biomedical Engineering, IEEE Transactions*, 58(10), 3016–3019.
- Walters, D. K., Burgreen, G. W., Hester, R. L., Thompson, D. S., Lavalley, D. M., Pruett, W. A., & Ford-Green, J. Simulations of Cyclic Breathing in the Conducting Zone of the Human Lung. *ASME Paper 2012*, No. FEDSM2012-72474. 2012.
- Weibel, E. R. (1963). *Morphometry of the human lung*. Berlin, Germany: Springer-Verlag.
- Zhang, Z., Kleinstreuer, C., & Kim, C. S. (2008). Airflow and nanoparticle deposition in a 16-generation tracheobronchial airway model. *Annals of Biomedical Engineering*, 36, 2095–2110.

Annex

Table I.A. Geometric dimensions of the lung branches.

Gen	Diameter (m)	Length (m)	Branches (m2)	Total (m2)
0	1.800000E-02	1.200000E-01	2.5447E-04	2.5447E-04
1	1.221142E-02	4.782228E-02	1.1712E-04	2.3424E-04
2	8.284380E-03	2.485314E-02	5.3903E-05	2.1561E-04
3	5.620225E-03	1.686068E-02	2.4808E-05	1.9847E-04
4	4.451270E-03	1.266542E-02	1.5562E-05	2.4899E-04
5	3.512926E-03	1.068537E-02	9.6923E-06	3.1015E-04
6	2.807205E-03	9.014874E-03	6.1893E-06	3.9611E-04
7	2.271429E-03	7.605532E-03	4.0522E-06	5.1868E-04
8	1.860991E-03	6.416519E-03	2.7201E-06	6.9634E-04
9	1.543866E-03	5.413392E-03	1.8720E-06	9.5847E-04
10	1.296864E-03	4.567088E-03	1.3209E-06	1.3526E-03
11	1.103061E-03	3.853092E-03	9.5563E-07	1.9571E-03
12	9.500025E-04	3.250718E-03	7.0883E-07	2.9033E-03
13	8.284568E-04	2.742516E-03	5.3905E-07	4.4159E-03
14	7.315347E-04	2.313764E-03	4.2030E-07	6.8862E-03
15	6.540636E-04	1.952042E-03	3.3599E-07	1.1010E-02
16	5.921409E-04	1.646869E-03	2.7538E-07	1.8048E-02